Synthesis and optical and magnetic property characterization of $Zn_{1-x-y}Co_xNi_yFe_2O_4$ (x & y= 0, 0.05, 0.15 and 0.25) nanoparticles

S. Yuvaraj [a], S. Ramachandran [b] , R. Sheela [b], R. Jothiramalingam [c*], R. S. R. Isaac [d], M. Sundararajan [e], S. Sasikumar [f]

[a] *Department of Physics, Vel Tech Rangarajan Dr. Sagunthala R&D Institute of Science and Technology, Vel Nagar, Avadi, Chennai-600 062, Tamil Nadu, India*

[b] *PG & Research Department of Physics, Arignar Anna College (Arts & Science), Krishnagiri-635115, Tamilnadu, India*

[c] *Chemistry Department, College of Science, King Saud University, P.O. Box.2455, Riyadh 11451, Saudi Arabia*

[d] *Department of Nanotechnology, Noorul Islam Centre for Higher Education, Kumaracoil, Kanyakumari 629180, Tamilnadu, India.*

[e] *PG & Research Department of Physics, Paavendhar College of Arts & Science, M.V. South, Thalaivasal, Salem, Tamil Nadu 636 121, India*

[f] *School of Materials Science and Engineering, Hunan University, Changsha, Hunan, 410082, China*

The synthesis of $Zn_{1-x-y}Co_xNi_yFe_2O_4$ ($0 \leq x$ & $y \leq 0.25$) nanoparticles has been carried out using a microwave combustion technique. The X-ray diffraction analysis of $ZnFe_2O_4$ samples, as well as $ZnFe_2O_4$ samples doped with Co^{2+} and Ni^{2+}, indicated the presence of a spinel structure with a crystallite size ranging from 11 to 29 nm. The lattice and crystallite were established using XRD analysis. The FE-SEM picture reveals a uniform grain morphology. The UV-Vis spectra indicated a rise in band gap values along with an increase in the concentration of Co^{2+} and Ni^{2+}. The VSM spectra demonstrate ferromagnetic behaviour in all of the samples.

(Received December 19, 2024; Accepted May 2, 2025)

Keywords: $ZnFe_2O_4$ spinel, Band gap, Crystallite size, Lattice parameter

1. Introduction

Innovative materials possessing these alluring qualities have transcended conventional materials with comparable attributes. Materials with the potential to be used in structural and optical applications include transition metal oxides with magnetic activity [1-3]. These ferrites have proven to be remarkably effective substitutes for a number of common systems with high nonlinearity. Zinc ferrite's propensity to absorb visible light and its photochemical stability have made it a great semiconductor photocatalyst. The remarkable magnetic properties of these materials have led to their widespread application in spintronic devices and magnetism. [4-6].

The properties of these materials have been observed to change as the grain size is reduced from a larger scale to the nanoscale. Bulk zinc ferrites generally display antiferromagnetic behaviour. However, when reduced to the nano regime, their magnetic characteristics can shift between being magnetically active and antiferromagnetic, depending on whether they form normal or inverted spinel structures. The findings obtained indicate that the primary magnetic characteristic of these zinc ferrites may be altered on a nanoscale level based on the different fabrication methods used.

*Corresponding author: rjothiram@gmail.com
https://doi.org/10.15251/JOR.2025.213.279

The variance in spinel structure is determined by the presence of zinc atoms occupying either the A-site or B-site. Remarkably, these $ZnFe_2O_4$ particles have shown an affinity for phosphates, hence enhancing their potential use in the removal of phosphates from water.

Introducing an external atom or element into the parent material may alter the characteristics and composition of the host material, as shown in previous studies on zinc ferrites doped with other metals. For instance, studies have revealed that changing the Zn:Co ratio can result in the formation of distorted spinel structures, as zinc and cobalt ferrites typically do not produce similar structures naturally [7]. Cobalt-doped zinc ferrite nanocomposites show improved microwave reflection loss across a wide frequency range [8]. In a magnesium-zinc ferrite system, nanofibers were found to be easily magnetizable, though their magnetic properties decreased with an increase in zinc content [9].

This work focuses on the synthesis of undoped zinc ferrite and Ni & Co doped zinc ferrite doped nanoparticles. Whether, electrons in the host are replaced by Co and Ni dopants, and the microwave combustion procedure was employed to create all of the samples. For samples with a pure phase, the dopant concentrations were limited to 100% under the experimental conditions. In order to ascertain their suitability for specific applications, they were further tested, and the best dopant for obtaining optical characteristics was identified.

2. Experimental

2.1. Materials preparation

The chemicals used in this study, namely zinc nitrate, cobalt nitrate, nickel nitrate, iron nitrate, and L-alanine, were all acquired from SD fine chemical in analytical grade. These compounds were used for synthesis without undergoing any further purification processes. The aforementioned chemical is used for the synthesis of nanoparticles of $Zn_{1-x-y}Co_xNi_yFe_2O_4$, where x and y range from 0.0 to 0.25. A homogenous mixture was created by taking the initial components zinc nitrate, cobalt nitrate, nickel nitrate, and iron nitrate in a mole ratio of 1:2. The pure $ZnFe_2O_4$ nanoparticles and the doped variants $Zn_{0.9}Co_{0.05}Ni_{0.05}Fe_2O_4$, $Zn_{0.9}Co_{0.15}Ni_{0.15}Fe_2O_4$, and $Zn_{0.9}Co_{0.25}Ni_{0.25}Fe_2O_4$ are designated as samples a, b, c, and d, respectively.

2.2. Techniques

This analysis was conducted using a Rigaku Ultima IV high-resolution X-ray powder diffractometer with a CuKα source (λ= 0.15418 nm), covering a 2θ range from 20° to 80°. Morphological and elemental analyses of the samples were carried out using a Joel JSM 6360 high-resolution scanning electron microscope, which includes a parallel energy dispersive X-ray spectrometer. Fluorescence analysis was conducted with a Perkin Elmer Is55, which identifies and quantifies emission peaks. Magnetic properties were assessed at 300K using a Lakeshore VSM 7410 model, featuring 3 Tesla magnets, with data recorded as magnetization (M) versus applied magnetic field (H).

3. Result and discussion

3.1. XRD analysis

The structural characteristics of synthesized pure $ZnFe_2O_4$ nanoparticles, along with those doped with Co and Ni, were examined using X-ray diffraction (XRD) analysis. The XRD patterns of the nanoparticles, as shown in Figure 1, include both pure $ZnFe_2O_4$ and Co and Ni doped $ZnFe_2O_4$. The diffraction peaks at angles of 30.09°, 35.25°, 36.84°, 42.90°, 53.37°, 56.65°, 62.28°, 64.01°, and 73.57°, corresponding to the indices 220, 311, 222, 400, 422, 511, 440, 531 and 533, align with the cubic spinel structure of zinc ferrite in the *Fd3m* space group, consistent with the JCPDS card No: 22-1012. Additionally, the presence of extra peaks at 24.15°, 32.21°, 35.56°, 40.87°, 49.47°, and 54.15°, indexed as 012, 104, 110, 113, 024, and 116, indicates the rhombohedral phase of Fe_2O_3, as confirmed by JCPDS card No: 80-2377. The crystallite sizes were determined to be 11, 16, 22, and 29 nm, respectively [16, 17].

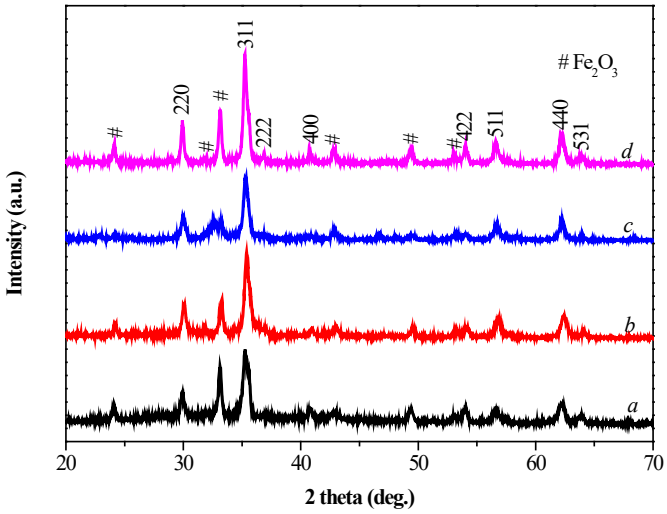

Fig. 1. XRD pattern of Co and Ni doped $ZnFe_2O_4$ nanoparticles.

The average crystallite size (L) was calculated using the given in equation (3).

$$L = \frac{0.89\lambda}{\beta \cos\theta} \tag{1}$$

where L represents the crystallite size, 0.89 is the Debye-Scherrer constant, λ denotes the X-ray wavelength, 2θ is the diffraction angle, and β is the full width at half maximum (FWHM) of the diffraction peak.

$$a^2 = d_{hkl}{}^2(h^2 + k^2 + l^2) \tag{2}$$

The inter-planer spacing, d_{hkl}, is determined by equation (1). It is associated with the Miller indices h, k, and l, d_{hkl} spacing, and lattice constant (a) are displayed in Table 1. The lattice parameter values exhibit a rising trend as the cobalt and nickel percentage values increase. This is due to the replacement of cobalt and nickel ions, which have greater ionic radii (200 and 163 pm, respectively), in the zinc ion sites (139 pm).

3.2. FE-SEM / EDX analysis

Figure 4 displays the SEM images of $ZnFe_2O_4$ nanoparticles that are pure, as well as doped with Co and Ni. The pure and zinc ferrite sample has a uniform and spherical grain morphology. Increasing the dopant concentration leads to the fragmentation of the grain shape. This impact is fully assimilated in all the samples.

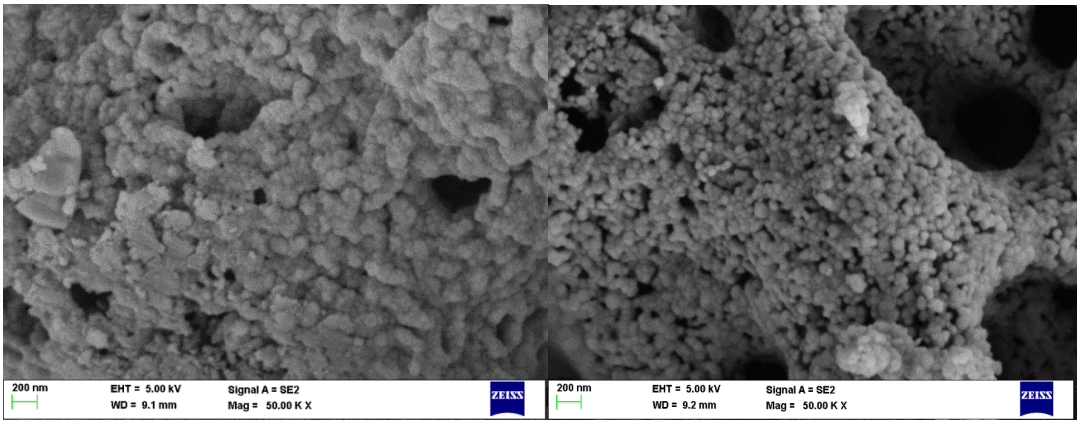

(a) *(b)*

Fig. 2. SEM analysis of Co and Ni doped $ZnFe_2O_4$ nanoparticles.

3.3. PL analysis

PL spectra were collected to learn more about sub-band gap, photogenerated charge carriers, and the emission process. The PL spectra were recorded at room temperature for all the samples and the excitation wavelength 414 nm are shown in Fig. 3. The emission peaks at 361 to 372 nm is due to the recombination of excited electrons and holes pairs. The emissions peaks are observed at 389 and 416 nm correspond to violet emissions caused by grain boundaries and oxygen for Co and Ni doped $ZnFe_2O_4$ nanoparticles [16]. Furthermore, as the increase the concentration of Co^{2+} and Ni^{2+} ions in the zinc ferrite, but the luminescence intensity decreases due to the recombination rate of electron-hole pairs [19].

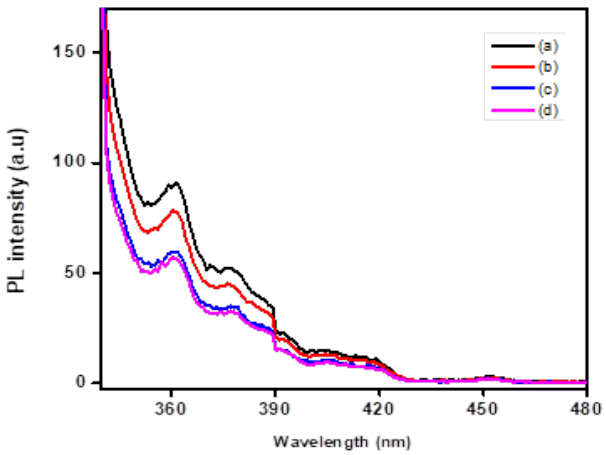

Fig. 3. PL analysis of Co and Ni doped $ZnFe_2O_4$ nanoparticles.

3.4. UV analysis

Spectra of diffuse reflectance were obtained for nanoparticles of $ZnFe_2O_4$ doped with Co and Ni. Applying the Kubelka-Munk function in conjunction with a modified Tauc relation. Figure 4 displays the linear segment of the figure depicting the relationship between hν and $(F(R)h\nu)^2$, as well as the expanded Y axis for all the Co and Ni doped zinc ferrite samples. When extrapolating the linear sections, the values of direct band gap may be obtained using the equation $(F(R)h\nu)^2 = 0$. The pronounced energy peaks observed in zinc ferrite nanoparticles result from electron transitions between fully occupied O-2p orbitals and vacant Fe-3d orbitals, representing the fundamental band-to-band transition. These peaks are closely related to the energy gap values. The Kubelka-

Munk (K-M) function, which is commonly used for powder samples, converts the absorption coefficient (α) as described in Eq. (3).

$$\alpha = \mathrm{F(R)} = \frac{(1-R)^2}{2R} \tag{3}$$

In this context, R represents reflectance, α denotes the absorption coefficient, and F(R) is the K-M function. The energy band gap values for cobalt and nickel-doped zinc ferrite are 1.97 eV and 1.75 eV, respectively. These values are lower than those reported in previous studies for zinc ferrite. The energy band gap may be affected by factors such as the surface area-to-volume ratio, microstructural defects, and particle size [13, 14].

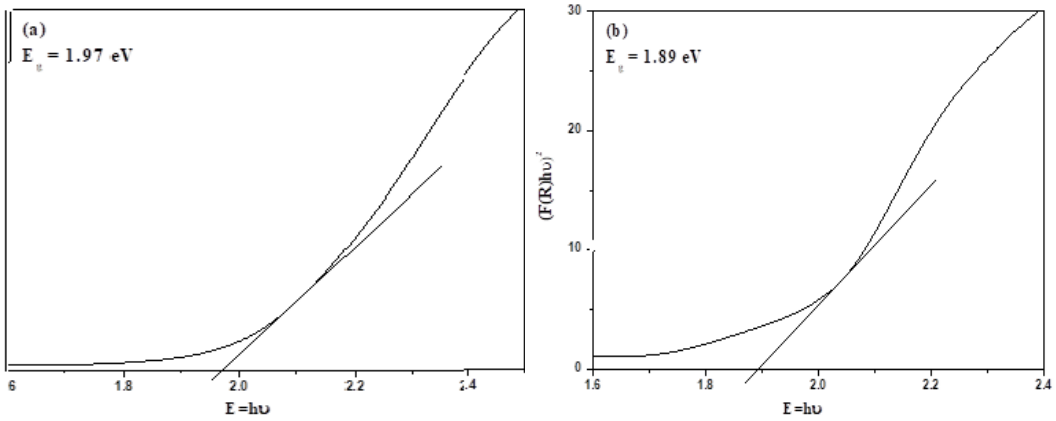

Fig. 4. DRS-UV analysis of Co and Ni doped $ZnFe_2O_4$ nanoparticles.

3.5. VSM analysis

The zinc ferrite nanoparticles exhibit ferromagnetic characteristics and reach saturation when exposed to a magnetic field within a specific range. The inclusion of non-magnetic Zn leads to a noticeable shift in both coercive and magnetization fields, suggesting that Zn^{2+} ions are incorporated into the iron lattice, influencing the magnetic exchange interactions between cations. The saturation magnetization and remanent magnetization (Mr) values range from 8.41 to 52.11 emu/g and 1.15 to 12.94 emu/g, respectively, while coercivity (Hc) values vary from 178.55 to 274.23 Oe (Table 1). These values demonstrate enhanced magnetic properties in $ZnFe_2O_4$ nanoparticles doped with Co and Ni, while still retaining the soft ferrite characteristics of zinc. The coercivity (Hc) is significantly influenced by factors such as anisotropy, temperature, particle size, dopants, and composition [14]. Additionally, increasing concentrations of Co and Ni ions have been shown to slightly increase lattice parameters.

Table 1. Magnetic properties of Co and Ni doped $ZnFe_2O_4$ spinel nanoparticles.

Sample	Sample code	Oe	M_r (emu/g)	M_s (emu/g)
$ZnFe_2O_4$	a	178.5	4.5	28.7
$Co_{0.05}Ni_{0.05}Zn_{0.9}Fe_2O_4$	b	192.5	1.1	8.4
$Co_{0.15}Ni_{0.15}Zn_{0.7}Fe_2O_4$	c	209.7	7.0	42.7
$Co_{0.25}Ni_{0.25}Zn_{0.5}Fe_2O_4$	d	274.2	12.9	52.1

4. Conclusion

The $Zn_{1-x-y}Co_xNi_yFe_2O_4$ ($0 \leq x$ & $y \leq 0.25$) nanoparticles were successfully synthesized using the direct microwave combustion method. The resulting samples of Co and Ni-doped $ZnFe_2O_4$ exhibit a cubic spinel structure with an *Fd3m* space group. Field emission scanning electron microscopy (FE-SEM) images showed a uniform grain morphology, while energy-dispersive X-ray (EDX) analysis detected only the Zn, Ni, Co, Fe, and O elements. The energy band gap values for the synthesized cobalt and nickel-doped zinc ferrite samples are 1.97 eV, 1.89 eV, 1.81 eV, and 1.75 eV, respectively. The incorporation of cobalt (Co) and nickel (Ni) into zinc ferrites improves their optical properties, making them highly suitable for optical device applications.

Acknowledgements

The author (Jothi Ramalingam Rajabathar) extend his appreciation and this work was funded by the Researchers Supporting Project Number (RSP2025R354) King Saud University, Riyadh, Saudi Arabia.

References

[1] Y. Koseoglu, A. Baykal, M.S. Toprak, F. Gozuak, A.C. Basaran, B. Aktas, J. Alloys Compd. 462 (2008) 209-213; https://doi.org/10.1016/j.jallcom.2007.07.121

[2] L. Satyanarayana, K.M. Reddy, S.V. Manorama, Sens. Actuators, B 89 (2003) 62-67; https://doi.org/10.1016/S0925-4005(02)00429-X

[3] J. Qiu, C. Wang, M. Gu, Mater. Sci. Eng., B 112 (2004) 1-4; https://doi.org/10.1016/j.mseb.2004.04.012

[4] H. Erhardt, S.J. Campbell, M. Hofman, J. Alloys Compd. 339 (2002) 255-260; https://doi.org/10.1016/S0925-8388(01)02011-4

[5] R. Kumar, A. Kumar, N. Verma, V. Khopkar, R. Philip, B. Sahoo, ACS Appl. Nano Mater. 3 (9) (2020) 8618-8631; https://doi.org/10.1021/acsanm.0c01284

[6] Lo Faro, Massimiliano, S.C. Zignani, A.S. Arico, Materials 13 (14) (2020) 3231; https://doi.org/10.3390/ma13143231

[7] T. Sofia Nirmala, N. Iyandurai, S. Yuvaraj, M. Sundararajan, Mater. Res. Express 7 (2020) 046104; https://doi.org/10.1088/2053-1591/ab7a7a

[8] Debasis Dhak, Panchanan Pramanik, J. Am. Ceram. Soc. 89 (2006) 1014-1021; https://doi.org/10.1111/j.1551-2916.2005.00769.x

[9] Y. Qiao, J. Xiao, Q. Jia, L. Lu, H. Fan, Results in Physics, 13 (2019) 102221; https://doi.org/10.1016/j.rinp.2019.102221

[10] R. Jothiramalingam, K. Mathankumar, M. Sundararajan, M. Sukumar, J. A. Dhanraj, R. Divya, H.A. Al-Lohedan, M. Chandrasekaran, D.M. Al-Dhayan, J. Ovonic Res. 18 (2022) 175.

[11] V.A. Bharati, Sandeep B. Somvanshi, Ashok V. Humbe, V.D. Murumkar, V. V. Sondur, K.M. Jadhav, J. Alloys Compd. 821 (2020), 15301; https://doi.org/10.1016/j.jallcom.2019.153501

[12] M. Sajjia, M. Oubaha, T. Prescott, A.G. Olabi, J. Alloys Compd. 506 (2010) 406; https://doi.org/10.1016/j.jallcom.2010.07.015

[13] S. Kanithan, N.A. Vignesh, K.M. Katubi, P.S. Subudhi, E. Yanmaz, J.A. Dhanraj, N. S. Alsaiari, M. Sukumar, M. Sundararajan, S. Baskar, S. Sahu, J. Mol. Struct. 1265 (2022), 133289; https://doi.org/10.1016/j.molstruc.2022.133289

[14] M. Sundararajan, A. Subramani, M. Ubaidullah, S.F. Shaikh, B. Pandit, S.K Jesudass, M. kamalakannan, S. Yuvaraj, P.S. Subudhi, Chandra Sekhar Dash, J. Cluster Sci.; https://doi.org/10.1007/s10876-022-02239-0